Structure and stability of arsenate adsorbed on α-Al$_2$O$_3$ single-crystal surfaces investigated using grazing-incidence EXAFS measurement and DFT calculation

Meiyi Zhang, Guangzhi He, Gang Pan*

Research Center for Eco-Environmental Sciences, Chinese Academy of Sciences, Beijing 100085, People's Republic of China

E-mail: myzhang@rcees.ac.cn, gzhhe@rcees.ac.cn, gpan@rcees.ac.cn

*Corresponding author. Phone: +86-10-62849686; Fax: +86-10-62849686; E-mail: gpan@rcees.ac.cn

1

Abstract: Direct characterization of contaminants on single-crystal planes is required because the specific adsorption characteristics on different exposed crystal planes constitute their actual behavior at water-mineral interfaces in aquifers. Here, the structure and stability of arsenate on α-Al$_2$O$_3$ (0001) and ($11\bar{2}0$) surfaces were characterized by using a combination of grazing-incidence extended X-ray absorption fine structure (GI-EXAFS) spectra and periodic density functional theory (DFT) calculation. The combined results indicated that arsenate was mainly adsorbed as inner-sphere monodentate and bidentate complexes on both surfaces, but the orientational polar angles on the (0001) surface were commonly 10~20° greater than that on the ($11\bar{2}0$) surface. The DFT calculation showed that the large polar angle was more favorable for arsenate stabilized on the alumina surfaces. Based on the spectroscopic and computational data, the dominant bonding modes of arsenate on the two crystal planes of α-Al$_2$O$_3$ were identified as bidentate binuclear structures, and the (0001) surface displayed a stronger affinity toward arsenate.

Keywords: surface complex; molecular orientation; structure-stability relationship; GI-EXAFS; density functional theory

1. Introduction

The persistence of arsenic in soil and aquatic environments has been ranked as a global environmental problem due to its toxic impact on human health (Oremland and Stolz, 2003). Adsorption of arsenic at the solid-water interface is one of the dominate effects responsible for water treatment and soil decontamination (Jing et al., 2005; Mohan and Pittman, 2007; Singer et al., 2013). Detailed information about the structure and stability of arsenic on solid surfaces is essential for understanding its fate in the environment and developing high-performance adsorbents (van Genuchten et al., 2012).

Over the past two decades, extended X-ray absorption fine structure (EXAFS) spectroscopy has been developed as one of the most important technologies for determining the microstructure of environmental contaminants on solid surfaces (Arai et al., 2001; Duarte et al., 2012; van Genuchten et al., 2012; Waychunas et al., 1993). Most existing EXAFS studies are carried out using powder substrates, where all types of crystal planes may be mixed and expose to the adsorption process. The multiple surface terminations and extensive defects of mineral powder may produce a large number of different adsorption sites (Daniels et al., 2001). Therefore, the structural data obtained from standard powder EXAFS experiment are essentially the average over all values from different exposed crystal planes. To avoid these problems, the application of structurally well-defined single-crystal substrates is needed (Catalano et al., 2005; Singer et al., 2012; Waychunas et al., 2005). Direct characterization of the structure and bonding properties on specific crystal planes is required to conclusively unveil the interaction of arsenic species with adsorbent powders.

Grazing-incidence EXAFS (GI-EXAFS) is a significant development of EXAFS technique, which utilizes well-characterized single-crystal samples (Singer et al., 2012). The application of

3

49 crystallographically anisotropic substrate and polarized X-ray beam allows GI-EXAFS to provide

50 more structural information (interatomic distance, coordination number and polar angle) toward the

51 oriented absorbates (Waychunas et al., 2005). These advantages provide the opportunity to obtain

52 direct information about the structure of contaminant molecules on different exposed crystal planes,

53 which may trigger wide applications of GI-EXAFS in environmental geochemistry and

54 geo-engineering as synchrotron facilities are improving. Density functional theory (DFT) calculation

55 can provide a detailed characterization of adsorbate molecules at solid surfaces, including structure,

56 bonding, and energy (Duarte et al., 2012; He et al., 2011). The combination of GI-EXAFS

57 measurement with DFT calculation enables analysis of the structure and stability characteristics of

58 arsenic species on specific crystal planes.

59 Aluminum is one of the most abundant metals in the earth, and Alumina has been recognized as a

60 very efficient adsorbent for the removal of arsenic from waters (Mohan and Pittman, 2007). α-Al_2O_3 is

61 the most stable phase of alumina with a well-determined structure, and an excellent model system for

62 understanding the transport mechanisms of contaminants on Al-(hydr)oxides (Catalano et al., 2008;

63 Trainor et al., 2001). Both (0001) and ($11\bar{2}0$) planes are stable terminations of α-Al_2O_3 surfaces

64 (Lockwood et al., 2008). However, there have been few studies of surface complexation reactions on

65 ($11\bar{2}0$) plane compared to (0001) and ($1\bar{1}02$) planes.

66 Here, we present a combined GI-EXAFS and DFT calculation investigation to study the structure

67 and stability of As(V) adsorbed on the (0001) and ($11\bar{2}0$) surfaces of α-Al_2O_3. In the GI-EXAFS

68 experiment, two directions of the X-ray electric vector, parallel and perpendicular to the substrate,

69 were used to determine the structure of As(V) bonded to both surfaces. Periodic DFT calculations

70 were performed to describe the binding and energetic characteristics of arsenate on α-Al_2O_3 surfaces.

2. Experimental and Computational Methods

2.1. Sample preparation

Highly polished $25 \times 25 \times 0.43$ mm^3 α-Al$_2$O$_3$ (0001) and ($11\bar{2}0$) single crystals were obtained commercially from Shanghai Daheng Optics and Fine Mechanics Co., Ltd, China. The orientations were checked using High accuracy X-ray single crystal orientation instrument (DX-4A, Dandong, China) and were found to be perfectly oriented to the resolution limits of the equipment (~2 Å). The roughness was assessed with AFM (Veeco Dimension 3100) and was found to be ≤5 Å rms. Prior to initial use, the crystals were washed in 10^{-4} mol/L nitric acid and ethanol followed by multiple rinses with MilliQ water (resistivity 18 MΩ.cm). The crystals were then equilibrated with 1 mmol/L Na$_2$HAsO$_4$ solution at pH 7.0 for 2h, with a 0.01 mol/L NaNO$_3$ background electrolyte. The pH of the reaction system was constantly monitored and adjusted to the desired value of 7.0 with 0.1 mol/L NaOH or 0.1 mol/L HNO$_3$. All chemicals used for solution preparation were of reagent grade quality.

2.2. GI-EXAFS data collection and analysis

Grazing-incidence EXAFS experiments were performed on the beamline BL14W1 at the Shanghai Synchrotron Radiation Facility (SSRF). A purposely built apparatus (Fig. S1 in the Supporting Information) consists of a carriage that holds the sample stage, with motor drives for positioning the sample over 5 degrees of freedom (Waychunas et al., 2005). A wet arsenate-loaded crystal sample was placed on the sample stage for GI-EXAFS measurements. The carriage can be rotated around the incident X-ray beam to set the angle of the X-ray electric vector polarization plane with respect to the sample surface. Ionization chamber detectors were mounted on both sides of the sample for transmission absorption data collection, and a 4-channel Si drift detector (SDD, Canberra Industries, Inc.) was used to collect fluorescence signals. The angle of the incident X-rays (beam diameter of ~30

93   μm) to the single-crystal surfaces was set to 0.16°, which is less than the critical angle of α-Al$_2$O$_3$ at

94   the energy position of As K-edge (0.19º) (Klockenkämper, 1997). The experimental uncertainty on the

95   incident angle of X-rays is ≤ 0.01°. The GI-EXAFS measurements were carried out using two scan

96   modes with the electric vector respectively parallel and perpendicular to the single-crystal substrate.

97   The crystal samples were mounted in a Teflon cell and sealed with Mylar film during the GI-EXAFS

98   experiment. During the data collection, the sample cell was continuously purged with a constant flow

99   of water-saturated inert gas (ultrapure N$_2$) to keep the crystals moist, which has been widely used in

100   GI-EXAFS experiments (Furnare et al., 2005; Waychunas et al., 2005). An average of 3 scans was

101   performed to achieve suitable single/noise, and no obvious change in spectral data was observed

102   during the 3 scans.

103   The spectral data were processed using WinXAS 3.1 software package (Ressler, 1998). A linear

104   function fit for the pre-edge region and a second-order polynomial fit in the post-edge region were

105   used to yield the normalized and background-corrected spectra. Subsequently, the normalized spectra

106   were converted to frequency (k) space using a cubic spline function and weighted by k^3. The k^{3}χ (k)

107   spectra (typically range from 2.2 to 12.4 Å^{-1}) were Fourier-transformed (FT) to R space using a Bessel

108   window function with smoothing parameter of 4. Theoretical phase shift and amplitude functions for

109   single- and multiple-scattering paths were calculated by ab initio Feff 9.0 code (Ankudinov et al.,

110   1998) using the cluster of scorodite (FeAsO$_4$·2H$_2$O) with the Fe atom replaced by Al atom. This

111   method has been successfully used in the study of arsenic species adsorption on Al-(hydr)oxide

112   surfaces (Arai et al., 2001). An amplitude reduction factor (S_0^2) of 0.9 was used in data-fitting

113   procedure (Grafe et al., 2008; Jing et al., 2005). We used 4, 2, and 1 as the starting values of the As-O

114   coordination number (CN_{As-O}), the CN_{As-Al} for binuclear complex, and the CN_{As-Al} for mononuclear

complex in the data fitting, to obtain estimated values for interatomic distances (R), DW factors σ^2, and ΔE_0. Then the R, σ^2, and ΔE_0 were fixed to obtain the estimated CN for each shell. The estimated values of CN, R, σ^2 and ΔE_0 were then used for a sequential fitting that recorded the reduction of the residual until the best fit was obtained. A single ΔE_0 was applied to all shells and allowed to float during the fitting. Finally, all the parameters (CN, R, σ^2) for each backscattering paths were allowed to vary. The goodness of fit is evaluated by the residual, defined as

$$\text{Residual [\%]} = \frac{\sum_{i=1}^{N} |y_{exp}(i) - y_{theo}(i)|}{\sum_{i=1}^{N} |y_{exp}(i)|} \cdot 100$$

with N the number of data points, y_{exp} and y_{theo} experimental and theoretical data points, respectively (Ressler, 2009). It has been reported that reasonable EXAFS results were generally obtained for arsenate adsorption on Fe- and Al-oxides when the residuals were less than 20% (Grafe and Sparks, 2005; Tang and Reeder, 2009). The As-Al shells were respectively regarded as a single shell and two subshells, and fitted using one single As-Al scattering path and two different As-Al paths. The results showed that the residuals of single-shell fits were commonly larger than that of two-subshell fits (see Fig. S2 in the Supporting Information), which experimentally confirmed the multiple coordination structures (i.e., the coexistence of two dominant adsorption configurations) of arsenate on α-Al_2O_3 surfaces. The experimental spectra were also fitted using the As-As scattering path and the As-O-O-As multiple scattering path (Fig. S3 and Fig. S4 in the Supporting Information). The increasing residuals indicated that the As(V)-bearing solid phase did not exist in the adsorption system considered here (1 mmol/L, pH 7.0), and no significant improvement was found by adding multiple scattering effects to the fitting. Therefore, to reduce the number of free parameters during the fitting, As-As scattering path and multiple scattering path were not employed in the final fitting.

2.3. Computational settings

The calculations were carried out using the generalized gradient approximation (GGA) with the functional parameterized by Perdew, Burke and Enzerhof (PBE) (Perdew et al., 1996) as implemented in the DMol3 module of Materials Studio package (Accerlys Software Inc.) (Delley, 1990; Delley, 2000). In the spin-restricted DFT calculations, the geometrical and electronic structures of Al-AsO$_4$ complexes were computed under periodic boundary conditions (PBC). The valence electron wave functions were expanded using a double numerical plus polarization (DNP) basis set which includes a polarized d-function for non-hydrogen atoms and p-function for hydrogen atoms (Delley, 2000). The size of the DNP basis set is comparable to Gaussian 6-31G (d, p), but the DNP is more accurate than a Gaussian basis set of the same size (Inada and Orita, 2008). The core electrons were described by effective core potentials (ECP) (Hay and Wadt, 1985). The global orbital cutoff was taken to be 4.8 Å (fine standard in DMol3). The conductor-like screening model (COSMO) was applied to simulate the water solvent environment (Klamt, 1995; Klamt and Schuurmann, 1993). The fine quality mesh size was employed for the numerical integration. The Brillouin zone was sampled with a 2×2×1 Monkhorst-Pack k-point grid for the structural optimization. A Fermi smearing of 0.005 hartree (1 hartree = 27.2114 eV = 2625.5 kJ/mol) was used to improve convergence efficiency (Delley, 1995). The geometry optimization convergence tolerances of the energy, gradient, and displacement were 1×10^{-5} Hartree, 2×10^{-3} Hartree Å^{-1}, and 5×10^{-3} Å, respectively.

2.4. Computational model

The unit cell of α-Al$_2$O$_3$ was optimized before construction of the supercell, and the calculated lattice constants (a = 4.759 Å, c = 12.991 Å) agreed favorably with the experimental values (a = 4.766 Å, c = 13.010 Å) and other theoretical works (Montanari et al., 2006). The surface in Fig. 1a is the

158 most stable among the three cleavage planes of α-Al$_2$O$_3$ (0001) surface (Mason et al., 2009; Walters et

159 al., 2000) and was used in this study. From existing studies, a slab contained five repeated Al$_2$O$_3$

160 layers generally allows a good description to the surface adsorption of adsorbate molecules (Duarte et

161 al., 2012; Hellman and Gronbeck, 2009). Therefore, the slab consisting of five Al$_2$O$_3$ layers was used

162 here as the surface model (see Fig. 1). The supercell expansions and spatial dimensions of each

163 surface slab are listed in Table 1. Surface hydroxylation of α-Al$_2$O$_3$ will occur in the presence of water,

164 and forms the reactive surface sites (Hass et al., 1998; Wang et al., 2000). Therefore, the surface of the

165 slab was hydroxylated in the calculation of arsenate surface complexation. During the geometrical

166 optimization, the arsenate and the top three Al$_2$O$_3$ layers (i.e., six atomic planes) were allowed to relax,

167 and the bottom two Al$_2$O$_3$ layers were fixed at equilibrium crystal lattice sites to simulate bulk

168 conditions (Hellman and Gronbeck, 2009; Ojamae et al., 2006; Ranea et al., 2008). A vacuum

169 thickness of 15 Å normal to the surface was used to eliminate spurious interactions between the

170 adsorbate and the periodic image of the bottom layer of the slabs (Roscioni et al., 2013). A counter

171 positive charge was automatically added by DMol3 package during the calculations in order to keep

172 the neutrality of the whole model to avoid divergence in the electrostatic energy (Makov and Payne,

173 1995).

a (0001)   **b** $(11\bar{2}0)$
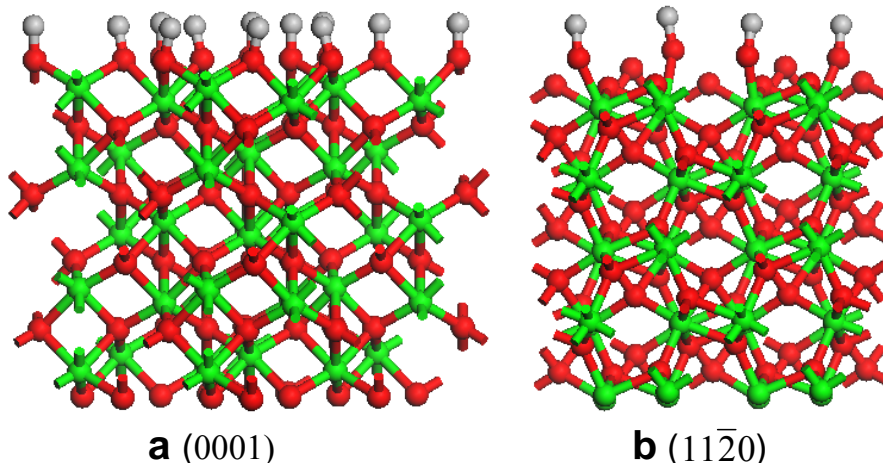
Fig. 1. Side views of the hydroxylated α-Al$_2$O$_3$ (0001) (a) and $(11\bar{2}0)$ (b) surface models used in DFT calculation. Green, red, and gray circles denote aluminum, oxygen, and hydrogen atoms, respectively.

Table 1. Supercell expansions and lattice parameters used to construct α-Al$_2$O$_3$ (0001) and $(11\bar{2}0)$ surface models

Surface	Expansion	L_x (Å)	L_y (Å)	L_z (Å)	Area/Å^2	N_{Al2O3}
(0001)	2×2	9.52	9.52	10.83	90.63	22
$(11\bar{2}0)$	1×2	7.00	10.26	11.17	71.82	20

Test calculations with larger orbital cutoff (5.2 Å) and denser k-point sampling (3×3×2) show almost no change in the structural and energetic properties. Negligible difference to the adsorption geometries (<0.01 Å) and binding energies (<5 kJ/mol) was found when the relaxed Al$_2$O$_3$ layers increased from 3 to 4 (see Table S1 in the Supporting Information), indicating that the structural parameters and relative energies of arsenate adsorption have converged when the relaxed Al$_2$O$_3$ layers increased to 3 (i.e., six atomic planes). These tests verified that the present computational settings and models were reliable for describing the properties of arsenate on α-Al$_2$O$_3$ surfaces.

3. Results and Discussion

3.1. GI-EXAFS analysis

10

188   The k^3-weighted and Fourier transform spectra of As K-edge GI-EXAFS for the adsorption samples

189   of arsenate on α-Al$_2$O$_3$ (0001) and (11$\overline{2}$0) single-crystal surfaces are shown in Fig. 2. GI-EXAFS

190   fitting data are presented in Table 2. Based on our fitting results, we estimated the accuracies of the

191   As–O shell to be ±0.005 Å for interatomic distance (R) and ±5% for coordination number (CN_{As-O}).

192   The estimated errors were ±0.02 Å, ±0.03 Å and ±20% for R of As–Al first subshell, R of As–Al

193   second subshell and $CN_{As–Al}$, respectively. The GI-EXAFS fitting results showed that the first

194   coordination shell of the arsenic atom consisted of four oxygen atoms at a distance of ~1.69 Å, which

195   is in good agreement with the literature (He et al., 2009; Waychunas et al., 2005). As a result of the

196   high symmetry of AsO$_4$ tetrahedron, no obvious difference in CN_{As-O} (Table 2) was observed between

197   both polarized scans (electric vector parallel and perpendicular to the substrate). For (0001) plane, the

198   two As-Al distances obtained from GI-EXAFS analysis (3.11±0.02 and 3.33±0.03 Å) agreed well with

199   DFT-calculated values of bidentate binuclear (BB) complex (3.07 Å) and monodentate binuclear (MB)

200   complex (3.30 Å), respectively (Table 3). The two experimentally measured As-Al distances on (11$\overline{2}$0)

201   plane (3.04±0.02 Å and 3.20±0.03 Å) were consistent with the theoretical values of BB (3.07 Å) and

202   monodentate mononuclear (MM, 3.21 Å) complexes (see Table 3).
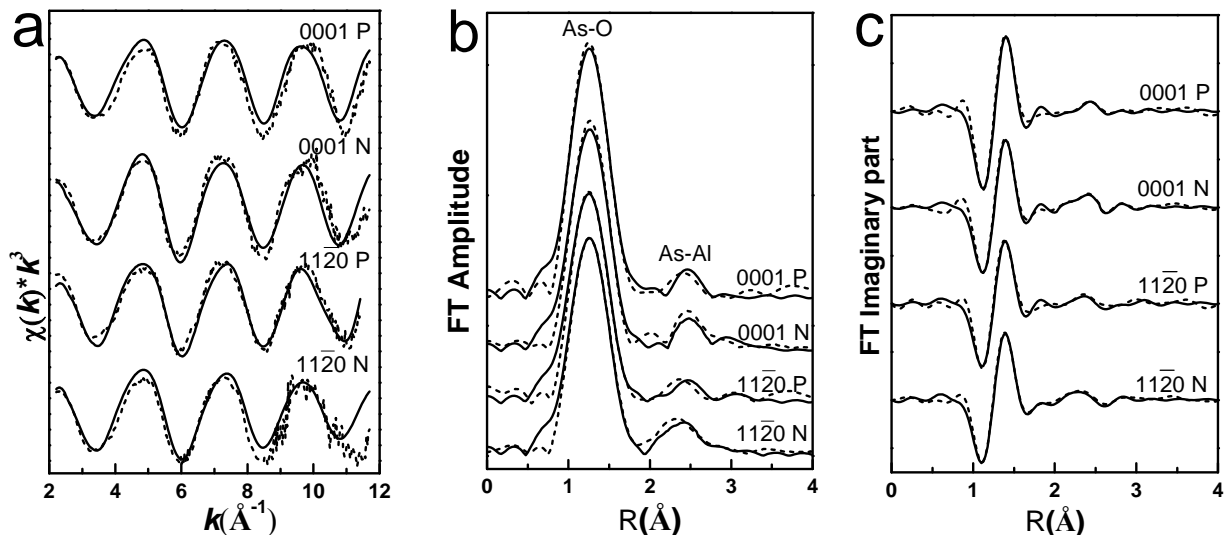
Fig. 2. (a) k^3-weighted GI-EXAFS, (b) Fourier transformed (FT) spectra, and (c) imaginary part of FT spectra of arsenate adsorption on α-Al$_2$O$_3$ (0001) and (11$\bar{2}$0) planes measured using two scan modes [electric vector parallel (P) and normal (N) to the substrate]. The dashed lines are the experimental spectra, while the solid lines are fitting curves. The peak positions are uncorrected for phase shifts.

Table 2. GI-EXAFS measured structural parameters of arsenate adsorption on α-Al$_2$O$_3$ (0001) and (11$\bar{2}$0) single-crystal planes*

Shell	Type of neighbor	CN	R(Å)	$DW(\sigma^2)$	ΔE_0(eV)	Residual*** (%)
(0001) surface E-vector						
First	O	4.0± 0.2	1.68± 0.005	0.002±0.001		
Second	Al	1.5± 0.3	3.11± 0.02	0.004±0.001	2.23	10.2
	Al	0.7± 0.2	3.32± 0.03	0.007±0.002		
(0001) surface E-vector normal						
First	O	4.0± 0.2	1.69± 0.005	0.003±0.001		
Second	Al	2.9± 0.6	3.12± 0.02	0.005±0.001	3.70	11.3
	Al	4.2± 0.8	3.35± 0.03	0.006±0.003		
(11$\bar{2}$0) surface E-vector parallel						
First	O	4.1± 0.2	1.68± 0.005	0.003±0.001		
Second	Al	1.4± 0.3	3.03± 0.02	0.005±0.002	3.45	11.4
	Al	0.4± 0.1	3.19± 0.03	0.007±0.003		
(11$\bar{2}$0) surface E-vector normal						
First	O	3.9± 0.2	1.69± 0.005	0.002±0.001	4.65	11.0
Second	Al	3.7± 0.7	3.05± 0.02	0.006±0.002		

12

	Al	2.6± 0.6	3.22± 0.03	0.006±0.003

210   * The listed parameters (*CN*, coordination number; *R*, interatomic distance; σ^2, Debye-Waller factor) reflected the

211   final best fit.

212   ** E-vector, electric vector.

213   *** Residual, gives a measure of the agreement between experimental and theoretical FT curves. All Residuals are <
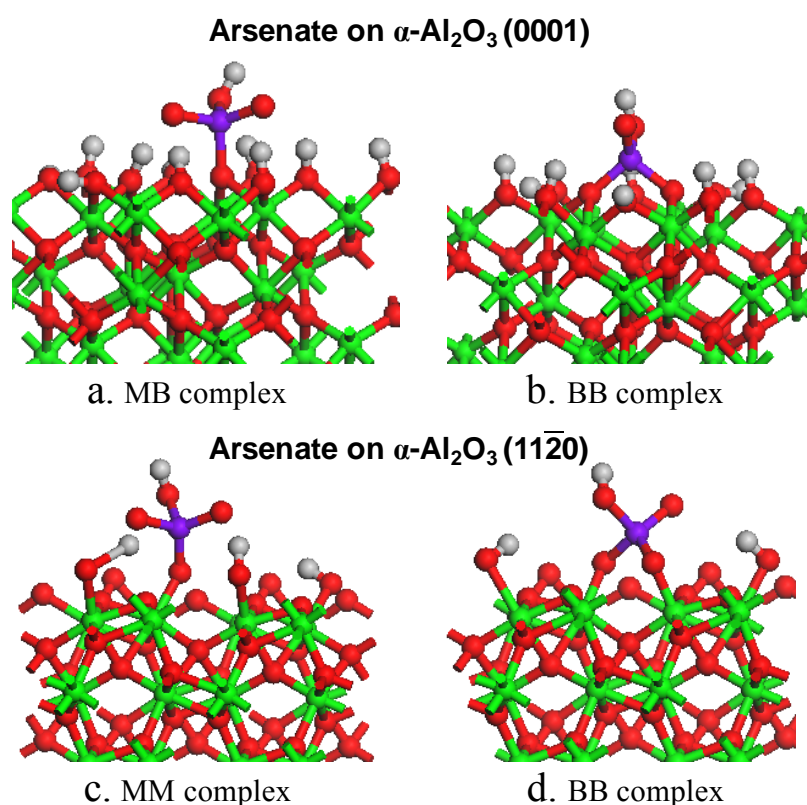
214   12%, indicating reliable fits.

215   An obvious difference in $CN_{As\text{-}Al}$ was observed from the same sample between the two scan modes

216   (see Table 2), resulting from the polarization dependence of As-Al bonds. Different to the CN_{iso}

217   determined by standard powder EXAFS, the polarized coordination number (CN_{pol}) obtained from

218   GI-EXAFS varies with the angle between the incident electric vector and the bond (Waychunas et al.,

219   2005). The polarization dependence allows a maximum of CN_{pol} when the bond parallel to the direction

220   of electric vector, and a near-zero value would appear when the bond normal to the electric vector in the

221   GI-EXAFS measurement. For instance, Fitts *et al.* presented that the CN_{pol} of Cu-Si bond on SiO_2 (0001)

222   surface in monodentate complex was 0.3 when the electric vector parallel to the substrate (Fitts et al.,

223   1999). It was also reported that a zero CN_{pol} value of Co-O bond occurred in an on-top complex of Co

224   (II) adsorbed on α-Al_2O_3 (0001) surface when the bond was absolutely normal to the electric vector

225   (Shirai et al., 1992; Shirai et al., 1994). The difference of $CN_{As\text{-}Al}$ between both polarized scans can be

226   used to deduce the polar angle (*ϕ*, angle between the As-Al vector and the substrate normal), and to

227   determine the stereostructure of each surface complex. For the two scan modes (electric vector parallel

228   and perpendicular to the support plane), the relationships between the coordination numbers of a

229   polarized EXAFS measurement (CN_{pol}) and that of isotropic EXAFS (CN_{iso}) are

230    $CN_{pol}^{\perp} = CN_{iso} \times 3\cos^2\phi$ and $CN_{pol}^{II} = \frac{3}{2}CN_{iso} \times \sin^2\phi$, respectively (Manceau et al., 2002; Waychunas

231   et al., 2005). Based on the two equations, the polar angles (*ϕ*) of BB complex obtained from GI-EXAFS

232   fitting were 45°±8° on (0001) surface and 36°±6° on ($11\bar{2}0$) surface, while the experimental *ϕ* of MB

233 complex on (0001) surface and MM complex on ($11\bar{2}0$) surface were 33°±8° and 18°±11° respectively.

234 The discrepancies between experimental and DFT-calculated polar angles (see Table 3) were less than

235 10°, indicating that a good estimation of the polar angles was obtained.

236 *3.2. DFT calculation*

237 $HAsO_4^{2-}$ is the dominant species of arsenate under pH 7.0 (i.e., the GI-EXAFS experimental condition)

238 (Sadiq, 1997), and hence was used in the DFT calculation to determine the adsorption site preference.

239 EXAFS signal is less influenced by the hydrogen atoms than by the heavier elements around the

240 absorbing atoms, and thus hydrogen atoms are normally not included in analyses of EXAFS data. Here,

241 we used DFT calculation to identify the protonation state of adsorbed arsenate. Monodentate binuclear

242 (MB) and bidentate binuclear (BB) complexes are the two typical structures of arsenate adsorbed on the

243 (0001) surface (see Fig. 3). On the ($11\bar{2}0$) surface, there are two kinds of unsaturated oxygen sites,

244 monodentate-terminal and bidentate-bridging O sites, which may be potentially formed the reactive sites.

245 Arsenate would be bonded as monodentate mononuclear (MM) and bidentate binuclear (BB) structures

246 at the terminal oxygen sites (Fig. 3), while a bidentate mononuclear (BM) adsorption mode may be

247 potentially produced at the bridging oxygen sites (Fig. S5a). However, the calculated BM adsorption

248 mode yielded an As-Al distance of 2.75 Å (see the Supporting Information), much smaller than the

249 distance obtained from experimental GI-EXAFS measurement, which confirmed the fact that the

250 twofold bridging oxygen site is less active than the high coordination-unsaturated terminal oxygen site

251 at the α-Al_2O_3 ($11\bar{2}0$) surface. Outer-sphere adsorption of arsenate on α-Al_2O_3 at pH 5 has been

252 reported (Catalano et al., 2008). It is well known that the surface complexation of arsenate on

253 metal-(hydr)oxides is significantly affected by pH. In our previous study of arsenate adsorption on

254 anatase TiO_2 surfaces (He et al., 2009), we also found that the as pH decreased to 5.5, outer-sphere

255 adsorption became thermodynamically favorable. However, there was no evidence indicating the

256 occurrence of outer-sphere adsorption of arsenate on α-Al$_2$O$_3$ surfaces under pH 7. Our DFT calculation

257 showed that the As-Al distances would be ~5 Å in outer-sphere Al-AsO$_4$ complexes (Fig. S5b), however,

258 no effective signals were observed more than 4 Å away from the As atom in the GI-EXAFS spectra (see

259 Fig. S2). Furthermore, outer-sphere H-bonded adsorption of arsenate on α-Al$_2$O$_3$ surfaces [e.g., -251.5

260 kJ/mol on (0001) surface] was more thermodynamically unfavorable than the inner-sphere adsorption

261 (-434.7 and -584.3 kJ/mol, see Table 3). This result indicated that arsenate adsorbed on the α-Al$_2$O$_3$

262 surfaces mainly as inner-sphere complexes under the neutral pH condition. Therefore, in order to

263 directly compare calculated results with experimental data, complexation at the bridging oxygen sites on

264 $(11\bar{2}0)$ surface and outer-sphere adsorption were excluded from the theoretical analysis and discussion.

Arsenate on α-Al$_2$O$_3$ (0001)

a. MB complex   b. BB complex

Arsenate on α-Al$_2$O$_3$ $(11\bar{2}0)$

c. MM complex   d. BB complex

265

266 **Fig. 3.** DFT-calculated structures of arsenate adsorbed on α-Al$_2$O$_3$ (0001) and $(11\bar{2}0)$ surfaces. Purple,

267 green, red, and gray circles denote arsenic, aluminum, oxygen, and hydrogen atoms, respectively.

268   Adsorption on the (0001) facet (-434.7 kJ/mol for monodentate complexes and -584.3 kJ/mol for

269   bidentate complexes) were generally energetically more favorable than that on the $(11\overline{2}0)$ facet

270   (-172.7 kJ/mol for monodentate complexes and -339.5 kJ/mol for bidentate complexes), indicating

271   that the (0001) facet exhibited a higher affinity toward arsenate. The spectral and computational

272   results showed that the polar angles of monodentate and bidentate complexes on the (0001) surface

273   were respectively 10~20°greater than that on the $(11\overline{2}0)$ surface (see Table 3). The result suggested

274   that a relatively large polar angle was more favorable for arsenate stabilized on α-Al$_2$O$_3$ surfaces. It

275   can be also noted that the DFT-calculated As-O distances for the Al-AsO$_4$ surface complexes (1.71 Å)

276   were generally slightly longer than the experimentally measured values (1.69 Å). This phenomenon

277   was also observed in the adsorption of arsenite on Fe-(hydr)oxides (Zhang et al., 2005). This

278   difference between experimental and theoretical values may be due to the theoretical underestimation

279   of solvent effect from COSMO model (Costentin et al., 2004; Tossell, 2005). However, we expect that

280   this artifact does not affect the relative stability of the adsorption modes and their complexation

281   properties.

282   **Table 3.** DFT-calculated interatomic distances (Å), polar angles (º) and binding energies (ΔE) of

283   arsenate adsorbed on α-Al$_2$O$_3$ surfaces

Bond	As-O(H)				Average	As- Al		Average	Polar angle*		Average	ΔE** (kJ/mol)
MB-(0001)-HAsO$_4$$^{2-}$	1.69	1.69	1.73	1.75	1.71	3.14	3.45	3.30	30	30	30	-434.7
BB-(0001)-HAsO$_4$$^{2-}$	1.69	1.71	1.72	1.74	1.71	2.98	3.17	3.07	42	40	41	-584.3
MM-$(11\overline{2}0)$-HAsO$_4$$^{2-}$	1.68	1.69	1.74	1.77	1.72	3.21	—	3.21	10	—	10	-172.7
BB-$(11\overline{2}0)$-HAsO$_4$$^{2-}$	1.69	1.70	1.72	1.75	1.71	3.01	3.13	3.07	33	30	32	-339.5

284   * Polar angle is the angle between the surface normal and the interatomic As-Ti vector direction.

16

285 ** ΔE were calculated as $\Delta E = E_{tot}$(Al-AsO$_4$)- [E_{tot}(arsenate) + E_{tot}(α-Al$_2$O$_3$)], where E_{tot}(Al-AsO$_4$) was the total energy
286 of Al-AsO$_4$ adsorption complex, E_{tot}(arsenate) and E_{tot}(α-Al$_2$O$_3$) were the total energy of arsenate molecule and
287 α-Al$_2$O$_3$ cluster, respectively. The structures of non-adsorbed arsenate were optimized in a periodic box with a side
288 length of 10 Å (Ojamae et al., 2006).

4. Conclusions

290 The spectral and computational results showed that arsenate primarily bonded as inner-sphere MB

291 and BB complexes on the (0001) surface of α-Al$_2$O$_3$, and MM and BB complexes on the ($11\bar{2}0$) surface.

292 The orientational polar angles on the (0001) surface were commonly 10~20° greater than that on the

293 ($11\bar{2}0$) surface for both monodentate and bidentate complexes. The DFT calculation showed that the

294 (0001) surface exhibited a stronger affinity toward arsenate, suggesting that the large polar angle was

295 more favorable for arsenate stabilization. The dominant bonding modes of arsenate on the two planes of

296 α-Al$_2$O$_3$ were identified as bidentate binuclear structures.

297 The combination of GI-EXAFS and DFT calculation facilitates the direct identification of adsorbed

298 species on different exposed crystal planes of the mineral. Our results demonstrated the arsenate

299 complexes on different crystal planes, which may be regarded as one single adsorption structure from

300 the measurements based on powder substrates, exhibited an obvious difference in stability. This

301 unambiguous characterization suggested a potential development to predict the fate and transport of

302 arsenic in aluminum-bearing soils, sediments, and water treatment systems that should take into account

303 the contributions from different crystal surfaces.

17

308   Academy of Sciences for providing access to the Materials Studio software.

309 **Appendix A. Supplementary data**

310 Supplementary data to this article can be found online at

311 **References**

312 Ankudinov, A. L., Ravel, B., Rehr, J. J., Conradson, S. D., 1998. Real-space multiple-scattering

313   calculation and interpretation of x-ray-absorption near-edge structure. Phys. Rev. B, 58(12):

314   7565-7576.

315 Arai, Y., Elzinga, E. J., Sparks, D. L., 2001. X-ray absorption spectroscopic investigation of arsenite

316   and arsenate adsorption at the aluminum oxide-water interface. J. Colloid Interface Sci., 235(1):

317   80-88.

318 Catalano, J. G., Park, C., Fenter, P., Zhang, Z., 2008. Simultaneous inner- and outer-sphere arsenate

319   adsorption on corundum and hematite. Geochim. Cosmochim. Acta, 72(8): 1986-2004.

320 Catalano, J. G., Trainor, T. P., Eng, P. J., Waychunas, G. A., Brown Jr, G. E., 2005. CTR diffraction and

321   grazing-incidence EXAFS study of U(VI) adsorption onto α-Al_2O_3 and α-Fe_2O_3 (1102)

322   surfaces. Geochim. Cosmochim. Acta, 69(14): 3555-3572.

323 Costentin, C., Robert, M., Saveant, J. M., 2004. Stepwise and concerted electron-transfer/bond

324   breaking reactions. Solvent control of the existence of unstable π ion radicals and of the

325   activation barriers of their heterolytic cleavage. J. Am. Chem. Soc., 126(51): 16834-16840.

326 Daniels, B. G., Lindsay, R., Thornton, G., 2001. A review of quantitative structural determinations of

327   adsorbates on metal oxide surfaces. Surf. Rev. Lett., 8(1-2): 95-120.

328 Delley, B., 1990. An all-electron numerical-method for solving the local density functional for

329   polyatomic-molecules. J. Chem. Phys., 92(1): 508-517.

330   Delley, B., 1995. DMol, a standard tool for density functional calculations: review and advances. In:

331   Seminario, J.M.P., P. (Ed.), Theoretical and Computational Chemistry. Elsevier, pp. 221-254.

332   Delley, B., 2000. From molecules to solids with the DMol(3) approach. J. Chem. Phys., 113(18):

333   7756-7764.

334   Duarte, G. et al., 2012. As(III) immobilization on gibbsite: investigation of the complexation

335   mechanism by combining EXAFS analyses and DFT calculations. Geochim. Cosmochim. Acta,

336   83: 205-216.

337   Fitts, J. P. et al., 1999. Grazing-incidence XAFS investigations of Cu(II) sorption products at

338   α-Al_2O_3-water and α-SiO_2-water interfaces. J. Synchrotron. Radiat., 6: 627-629.

339   Furnare, L. J., Vailionis, A., Strawn, D. G., 2005. Polarized XANES and EXAFS spectroscopic

340   investigation into copper(II) complexes on vermiculite. Geochim. Cosmochim. Acta, 69(22):

341   5219-5231.

342   Grafe, M., Sparks, D. L., 2005. Kinetics of zinc and arsenate co-sorption at the goethite-water

343   interface. Geochim. Cosmochim. Acta, 69(19): 4573-4595.

344   Grafe, M., Tappero, R. V., Marcus, M. A., Sparks, D. L., 2008. Arsenic speciation in multiple metal

345   environments: I. Bulk-XAFS spectroscopy of model and mixed compounds. J. Colloid

346   Interface Sci., 320(2): 383-399.

347   Hass, K. C., Schneider, W. F., Curioni, A., Andreoni, W., 1998. The chemistry of water on alumina

348   surfaces: Reaction dynamics from first principles. Science, 282(5387): 265-268.

349   Hay, P. J., Wadt, W. R., 1985. Abinitio effective core potentials for molecular calculations - potentials

350   for K to Au including the outermost core orbitals. J. Chem. Phys., 82(1): 299-310.

351 He, G., Pan, G., Zhang, M., 2011. Studies on the reaction pathway of arsenate adsorption at water-TiO_2

352   interfaces using density functional theory. J. Colloid Interface Sci., 364(2): 476-481.

353 He, G., Zhang, M., Pan, G., 2009. Influence of pH on initial concentration effect of arsenate adsorption

354   on TiO_2 surfaces: thermodynamic, DFT, and EXAFS Interpretations. J. Phys. Chem. C,

355   113(52): 21679-21686.

356 Hellman, A., Gronbeck, H., 2009. First-Principles Studies of NO_x Chemistry on Ag_n/α-Al_2O_3. J. Phys.

357   Chem. C, 113(9): 3674-3682.

358 Inada, Y., Orita, H., 2008. Efficiency of numerical basis sets for predicting the binding energies of

359   hydrogen bonded complexes: Evidence of small basis set superposition error compared to

360   Gaussian basis sets. J. Comput. Chem., 29(2): 225-232.

361 Jing, C., Liu, S., Patel, M., Meng, X., 2005. Arsenic leachability in water treatment adsorbents.

362   Environ. Sci. Technol., 39(14): 5481-5487.

363 Klamt, A., 1995. Conductor-like screening model for real solvents - a new approach to the quantitative

364   calculation of solvation phenomena. J. Phys. Chem., 99(7): 2224-2235.

365 Klamt, A., Schuurmann, G., 1993. Cosmo - a new approach to dielectric screening in solvents with

366   explicit expressions for the screening energy and its gradient. J. Chem. Soc., Perkin Trans. 2(5):

367   799-805.

368 Klockenkämper, R., 1997. Total reflection X Ray Fluorescence Analysis. Wiley, New York

369 Lockwood, G. K., Zhang, S. H., Garofalini, S. H., 2008. Anisotropic dissolution of α-Alumina (0001)

370   and (1120) surfaces into adjoining silicates. J. Am. Ceram. Soc., 91(11): 3536-3541.

371 Makov, G., Payne, M. C., 1995. Periodic boundary-conditions in ab-Initio calculations. Phys. Rev. B,

372   51(7): 4014-4022.

373 Manceau, A., Lanson, B., Drits, V. A., 2002. Structure of heavy metal sorbed birnessite. Part III:

374   Results from powder and polarized extended X-ray absorption fine structure spectroscopy.

375   Geochim. Cosmochim. Acta, 66(15): 2639-2663.

376 Mason, S. E., Iceman, C. R., Tanwar, K. S., Trainor, T. P., Chaka, A. M., 2009. Pb(II) Adsorption on

377   Isostructural Hydrated Alumina and Hematite (0001) Surfaces: A DFT Study. J. Phys. Chem. C,

378   113(6): 2159-2170.

379 Mohan, D., Pittman, C. U., Jr., 2007. Arsenic removal from water/wastewater using adsorbents - A

380   critical review. J. Hazard. Mater., 142(1-2): 1-53.

381 Montanari, B., Civalleri, B., Zicovich-Wilson, C. M., Dovesi, R., 2006. Influence of the

382   exchange-correlation functional in all-electron calculations of the vibrational frequencies of

383   corundum (α-Al_2O_3). Int. J. Quantum Chem., 106(7): 1703-1714.

384 Ojamae, L., Aulin, C., Pedersen, H., Kall, P. O., 2006. IR and quantum-chemical studies of carboxylic

385   acid and glycine adsorption on rutile TiO_2 nanoparticles. J. Colloid Interface Sci., 296(1):

386   71-78.

387 Oremland, R. S., Stolz, J. F., 2003. The ecology of arsenic. Science, 300(5621): 939-944.

388 Perdew, J. P., Burke, K., Ernzerhof, M., 1996. Generalized Gradient Approximation Made Simple.

389   Phys. Rev. Lett., 77(18): 3865-3868.

390 Ranea, V. A., Schneider, W. F., Carmichael, I., 2008. DFT characterization of coverage dependent

391   molecular water adsorption modes on α-Al_2O_3(0001). Surf. Sci., 602(1): 268-275.

392 Ressler, T., 1998. WinXAS: a program for X-ray absorption spectroscopy data analysis under

393   MS-Windows. J. Synchrot. Radiat., 5(2): 118-122.

394 Ressler, T., 2009. Manual WinXAS. Version 3.x,1992-2009. Department of Inorganic Chemistry.

395   Germany.

396   Roscioni, O. M., Dyke, J. M., Evans, J., 2013. Structural characterization of supported

397        $Rh^I(CO)_2/\gamma$-Al_2O_3 catalysts by periodic DFT calculations. J. Phys. Chem. C, 117(38):

398   19464-19470.

399   Sadiq, M., 1997. Arsenic chemistry in soils: An overview of thermodynamic predictions and field

400   observations. Water Air Soil Poll, 93(1-4): 117-136.

401   Shirai, M., Asakura, K., Iwasawa, Y., 1992. Anisotropic structure-analysis for cobalt oxides on

402   α-Al_2O_3 (0001) by polarized total-reflection fluorescence extended X-ray absorption

403   fine-structure. Catal. Lett., 15(3): 247-254.

404   Shirai, M., Inoue, T., Onishi, H., Asakura, K., Iwasawa, Y., 1994. Polarized total-reflection

405   rluorescence exafs study of anisotropic structure-analysis for Co oxides on α-Al_2O_3 (0001) as

406   model surfaces for active oxidation catalysts. J. Catal., 145(1): 159-165.

407   Singer, D. M. et al., 2012. Identification of Simultaneous U(VI) Sorption Complexes and U(IV)

408   Nanoprecipitates on the Magnetite (111) Surface. Environ. Sci. Technol., 46(7): 3811-3820.

409   Singer, D. M., Fox, P. M., Guo, H., Marcus, M. A., Davis, J. A., 2013. Sorption and redox reactions of

410   As(III) and As(V) within secondary mineral coatings on aquifer sediment grains. Environ. Sci.

411   Technol., 47(20): 11569-11576.

412   Tang, Y. Z., Reeder, R. J., 2009. Uranyl and arsenate cosorption on aluminum oxide surface. Geochim.

413   Cosmochim. Acta, 73(10): 2727-2743.

414   Tossell, J. A., 2005. Theoretical study on the dimerization of $Si(OH)_4$ in aqueous solution and its

415   dependence on temperature and dielectric constant. Geochim. Cosmochim. Acta, 69(2):

416   283-291.

417 Trainor, T. P., Fitts, J. P., Templeton, A. S., Grolimund, D., Brown, G. E., 2001. Grazing-incidence

418 XAFS study of aqueous Zn(II) sorption on α-Al_2O_3 single crystals. J. Colloid Interface Sci.,

419 244(2): 239-244.

420 van Genuchten, C. M., Addy, S. E. A., Pena, J., Gadgil, A. J., 2012. Removing arsenic from synthetic

421 groundwater with iron electrocoagulation: an Fe and As K-Edge EXAFS study. Environ. Sci.

422 Technol., 46(2): 986-994.

423 Walters, C. F., McCarty, K. F., Soares, E. A., Van Hove, M. A., 2000. The surface structure of α-Al_2O_3

424 determined by low-energy electron diffraction: aluminum termination and evidence for

425 anomolously large thermal vibrations. Surf. Sci., 464(2-3): L732-L738.

426 Wang, X. G., Chaka, A., Scheffler, M., 2000. Effect of the environment on α-Al_2O_3 (0001) surface

427 structures. Phys. Rev. Lett., 84(16): 3650-3653.

428 Waychunas, G. et al., 2005. Surface complexation studied via combined grazing-incidence EXAFS

429 and surface diffraction: arsenate on hematite (0001) and (1012). Anal. Bioanal. Chem., 383(1):

430 12-27.

431 Waychunas, G. A., Rea, B. A., Fuller, C. C., Davis, J. A., 1993. Surface-chemistry of Ferrihydrite .1.

432 EXAFS studies of the geometry of coprecipitated and adsorbed arsenate. Geochim.

433 Cosmochim. Acta, 57(10): 2251-2269.

434 Zhang, N. L., Blowers, P., Farrell, J., 2005. Evaluation of density functional theory methods for

435 studying chemisorption of arsenite on ferric hydroxides. Environ. Sci. Technol., 39(13):

436 4816-4822.

437

438